LOCAL OXYGEN GRADIENTS NEAR ISOLATED MITOCHONDRIA

ALFRED CLARK, JR. AND PATRICIA A. A. CLARK
Department of Mechanical Engineering, University of Rochester, Rochester, New York 14627; and Department of Mathematics, Rochester Institute of Technology, Rochester, New York 14623

ABSTRACT The oxygen concentration in tissue can vary on several length scales. The basic scale of variation is determined by capillary spacing. It is this scale that is manifest in the simplest Krogh cylinder model. A second, smaller scale of variation is associated with the consumption of oxygen by mitochondria. This paper gives a theoretical analysis of these smaller-scale oxygen variations near an isolated mitochondrion. To illustrate the effects of shape, we have carried out the calculations for prolate spheroids as well as for spheres. The principal result is that the local drop in oxygen pressure around a consuming mitochondrion is of the order of $(\Gamma/3K)\ (3V/4\pi)^{2/3}$, where Γ is the oxygen consumption rate per unit mitochondrial volume, K is the Krogh oxygen diffusivity of the surrounding tissue, and V is the mitochondrial volume. The theory is applied to skeletal muscle in vivo and to hepatocytes in cell suspension experiments. In both cases, we find that local oxygen variations produced by oxygen consumption are much smaller than the cell-wide variations produced by the collective effect of all the mitochondria. For example, in maximally consuming skeletal muscle, the drop in oxygen pressure around a consuming mitochondrion is only of the order of 0.03 Torr.

INTRODUCTION

In the model of oxygen transport pioneered by Krogh (1922), a cylinder of tissue, supplied by a central capillary, consumes oxygen uniformly throughout its volume. In this picture, the scale of spatial variation of oxygen concentration is of the order of the Krogh cylinder diameter, a length comparable to the cell diameter. This is the only scale of variation in the simplest Krogh model. Because the actual oxygen consumption in tissue is not uniform, but occurs in mitochondria, there will exist a second, smaller scale of variation, corresponding to the mitochondrial size. The oxygen distribution calculated from the Krogh model can be thought of as a kind of large-scale approximation, in which the actual distribution is averaged over a scale larger than the mitochondrial diameter but smaller than the cell diameter. In this averaged description, the individual mitochondria are replaced by a smooth (usually uniform) distribution of oxygen sinks. The actual oxygen distribution can then be thought of as a superposition of this large-scale distribution and the local (small-scale) variations associated with mitochondria. A number of authors (Tamura et al., 1978; Fletcher, 1980; de Konig et al., 1981; Jones and Kennedy, 1982; Kreuzer and Hoofd, 1984) have suggested that the perimitochondrial gradients are steep. The objective of this paper is to test this idea by giving a detailed theoretical description of these gradients.

The analysis presented here allows one to deal with several questions of physiological interest, including the following: (*a*) Are the local drops in P_{O_2} around individual mitochondria large enough to be observed? (*b*) Are the cytochromes in an oxygen-consuming mitochondrion exposed to a P_{O_2} that is lower than that of the nearby tissue? (*c*) By how much does P_{O_2} vary on the mitochondrial surface? (*d*) In modeling oxygen transport to tissue, can we ignore individual mitochondria and just deal with the large-scale oxygen distribution?

The mathematical treatment of the problem is given in the Analysis section. First, the basic assumptions of the model are discussed, with an emphasis on questions of mitochondrial geometry. Then the problem for an isolated mitochondrion is formulated and solved. The spherical case is done first, because it is sufficiently simple to show how the oxygen gradients depend on the parameters of the problem. As a more realistic model, we also examine the case of a prolate spheroid. The results for spheroids are presented in the form of shape factors, which relate the spheroids to spheres of equal volume. The final part of the Analysis section gives a summary of the results. The mathematical details for the prolate spheroidal case are given in the Appendix. Some related earlier theoretical work is that of Bouwer and van den Thillart (1984), who calculated oxygen gradients around spherical mitochondria in suspension.

In the Applications section of the paper, the theory is applied to two examples: skeletal muscle and hepatocyte suspensions. In both cases, the theoretical results are compared with relevant experiments.

GLOSSARY

a	radius of spherical mitochondrion (cm)
B	oxygen solubility coefficient (mol/cm^3 · Torr)
b	minor semi-axis of prolate spheroid (cm)

C	local drop in oxygen pressure caused by mitochondrial oxygen consumption (Torr)
c	major semi-axis of prolate spheroid (cm)
C_C	value of C at mitochondrial center (Torr)
C_I	value of C inside mitochondrion (Torr)
C_O	value of C outside mitochondrion (Torr)
$\langle C \rangle_A$	average of C on mitochondrial surface (Torr)
$\langle C \rangle_V$	average of C in mitochondrial volume (Torr)
D	oxygen diffusivity (cm^2/s)
$\mathbf{F}$	large-scale oxygen gradient at mitochondrion (Torr/cm)
F_m	volume fraction of mitochondria
G	geometrical factor; 4 for cylinder, 6 for sphere
$K = BD$	Krogh diffusivity (mol/cm · s · Torr)
$\mathbf{n}$	unit normal to mitochondrial surface
P	oxygen partial pressure (Torr)
P_C	P at center of mitochondrion (Torr)
P_I	P inside mitochondrion (Torr)
P_O	P outside mitochondrion (Torr)
P_∞	value of large-scale P at mitochondrion (Torr)
$P_\bullet$	reference value of P (Torr)
$\langle P \rangle_A$	average of P on mitochondrial surface (Torr)
$\langle P \rangle_V$	average of P in mitochondrial volume (Torr)
$(\Delta P)_{CELL}$	variation of P across cell (Torr)
$(\Delta P)_{MITO}$	variation of P near mitochondrion (Torr)
$R = b/c$	axis ratio of prolate spheroid
R_c	cell radius (cm)
$\mathbf{r}$	position vector (cm)
r	magnitude of $\mathbf{r}$ (cm)
S_A	shape factor for $\langle C \rangle_A$
S_C	shape factor for C_C
S_V	shape factor for $\langle C \rangle_V$
V	volume of mitochondrion (cm^3)
x, y, z	Cartesian coordinates (cm)
Γ	oxygen consumption rate inside mitochondrion (mol/cm^3 · s)
$\Gamma_c = \Gamma F_m$	cell oxygen consumption rate (mol/cm^3 · s)

ANALYSIS

Assumptions

The most difficult issue in modeling oxygen transport to mitochondria is the mitochondrial geometry. Pictures in the literature exhibit an enormous variety of mitochondrial shapes and distributions. It is useful to introduce three geometric prototypes: (*a*) a distribution of isolated mitochondria of fairly regular shape, (*b*) a distribution of long columns of mitochondria of fairly regular cross section, and (*c*) distributions of mitochondria with complex or irregular shapes (e.g., mitochondria with many branching processes, or complex, nonconvex cross sections). The theories associated with these cases are quite different. In case *a*, which is dealt with in the present paper, there is a clear separation between the oxygen variations on the larger cellular scale, and the local mitochondrial variations. In case *b*, which we plan to deal with in a future work, the problem is still tractable, but the large-scale and small-scale variations are not so cleanly separated. Case *c* will require a statistical theory, in addition to the insight gained from cases *a* and *b*. Although no real tissue fits case *a* or *b* exactly, some examples come close. Electron micrographs of hepatocytes, for example, often show mitochondrial geometry that approaches case *a*. Insect flight muscles and cardiac muscle are good examples of case *b*. Some tissues are intermediate between case *a* and case *b*. In dog gracilis muscle, for example, the mitochondria are in a columnar arrangement, but there are gaps, with many mitochondria being isolated and with some touching their neighbors. It is not unreasonable to apply the theory of case *a* to such a tissue. Since the oxygen drops produced by individual mitochondria are superposable, we can deal with the case of touching mitochondria by adding the drops for each, calculated on the basis of case *a*. Roughly speaking, the maximum oxygen drop in the vicinity of two touching mitochondria will be twice the drop for an isolated mitochondrion. In the remainder of this paper, we deal only with isolated mitochondria in the shape of spheres or prolate spheroids.

The calculation of the local oxygen variations for isolated mitochondria is based on the two-scale concept discussed in the Introduction. The underlying assumption is that the mitochondrial scale is much smaller than the cell scale. This is well-satisfied for skeletal muscle and hepatocytes, the two cases to which we apply the theory in this paper. In both cases, the cell diameter is of the order of 50 times the mitochondrial diameter.

The Krogh oxygen diffusivity is an important parameter in the problem. Although we have carried out extensive calculations for the case in which the diffusivity inside the mitochondrion differs from the diffusivity in the surrounding tissue, we present here only the simpler case, when the two are equal. Our more general calculations show that the oxygen gradients outside the mitochondrion are determined largely by the tissue diffusivity and are not sensitive to the value of the ratio of the mitochondrial to tissue diffusivity. In any case, there seems to be no experimental evidence that the diffusivities differ greatly.

A second important parameter in the problem is the oxygen consumption rate within the mitochondrion. Once again, we make a simplifying assumption and take the rate to be uniform. Again, the oxygen gradients outside the mitochondrion are not very sensitive to this assumption, since those gradients depend mostly on the total oxygen consumption of the mitochondrion, and only weakly on the distribution of consumption sites within the mitochondrion.

Formulation

The physical quantities that we deal with (and their units) are as follows: oxygen concentration N (mol/cm^3), oxygen diffusivity D (cm^2/s), oxygen solubility coefficient B (mol/cm^3 · Torr), Krogh oxygen diffusivity $K = BD$ (mol/cm · s · Torr), oxygen partial pressure P (Torr), with $N = BP$, and oxygen consumption rate per unit volume of mitochondrial tissue Γ (mol/cm^3 · s). As discussed above, we take Γ to be constant, and K to be uniform inside and outside the mitochondrion. We consider an isolated mitochondrion occupying a volume V_I, bounded by a surface A, and we denote the volume of tissue exterior to the mitochondrion

by V_O. We use subscripts I and O, when necessary, to distinguish quantities inside and outside the mitochondrion. Then the steady state oxygen balance inside the mitochondrion is

$$\nabla^2 P_I = \Gamma/K. \tag{1}$$

In the tissue region outside the mitochondrion, the oxygen balance is simply

$$\nabla^2 P_O = 0. \tag{2}$$

In Eq. 2, we are ignoring any carrier proteins, such as myoglobin, in the tissue. (A brief discussion of the effects of myoglobin will be given later.) On the mitochondrial surface A, the oxygen flux must be continuous, and, in the absence of any significant membrane resistance, the oxygen partial pressure must be continuous. Hence we have

$$P_I = P_O, \quad \text{and } \mathbf{n} \cdot \nabla P_I = \mathbf{n} \cdot \nabla P_O \quad \text{on } A. \tag{3}$$

The next step in the formulation is to specify the conditions far from the mitochondrion. This involves a knowledge of the large-scale oxygen field in which the mitochondrion is embedded. We let P_∞ be the value of the large-scale field at the centroid of the mitochondrion, and we let $\mathbf{F}$ be the value of the large-scale field gradient at the same point. Then the asymptotic condition on the local field is

$$P_O - P_\infty \sim \mathbf{F} \cdot \mathbf{r} \quad \text{as } r \to \infty. \tag{4}$$

Here $\mathbf{r}$ is the position vector, and $r = |\mathbf{r}|$. A more formal development going beyond Eq. 4 may be based on a Taylor series expansion of the large-scale oxygen field about the centroid of the mitochondrion. Such a treatment amounts to an expansion in powers of a small parameter—namely, the ratio of the mitochondrial scale to the cell scale. The terms in Eq. 4 are sufficient for our purposes here, so we do not need to carry out the formal expansion scheme.

As a last step in the formulation, we introduce explicitly the oxygen pressure drop C associated with the mitochondrial oxygen consumption

$$P = P_\infty + \mathbf{F} \cdot \mathbf{r} - C. \tag{5}$$

The consumption part C then satisfies

$$\nabla^2 C_I = -\Gamma/K, \quad \nabla^2 C_O = 0, \tag{6}$$

$$C_I = C_O, \quad \mathbf{n} \cdot \nabla C_I = \mathbf{n} \cdot \nabla C_O \quad \text{on } A, \tag{7}$$

and

$$C_O \to 0 \quad \text{as } r \to \infty. \tag{8}$$

Solution

The function $C(\mathbf{r})$, defined by Eqs. 6–8, is the value at $\mathbf{r}$ of the drop in oxygen pressure (below P_∞) caused by the oxygen consumption. We calculate C, first for a sphere and then for a family of prolate spheroids. We have chosen to characterize the solution by the following quantities: (*a*) C_C, the value of C at the center of the mitochondrion; (*b*) $\langle C \rangle_V$, the value of C averaged over the volume of the mitochondrion; (*c*) $\langle C \rangle_A$, the value of C averaged over the surface of the mitochondrion.

Consider a spherical mitochondrion of radius a. We put the coordinate origin at the center of the sphere, and we let r be the spherical radial coordinate. Then the solution of Eqs. 6–8 is straightforward, and we obtain

$$C_I = P_\bullet[1 + (\tfrac{1}{2})(1 - r^2/a^2)], \quad C_O = P_\bullet(a/r), \tag{12}$$

where $P_\bullet = \Gamma a^2/(3K)$ is the basic scale for the oxygen pressure drop. For purposes of comparison with the spheroidal case, it is more useful to express $P_\bullet$ in terms of the volume V of the sphere rather than the radius a:

$$P_\bullet = (\Gamma/3K)(3V/4\pi)^{2/3}. \tag{13}$$

From Eqs. 12 and 13, we calculate

$$C_C = (3/2)P_\bullet, \quad \langle C \rangle_A = P_\bullet,$$

and

$$\langle C \rangle_V = (6/5)P_\bullet \quad \text{(sphere)}. \tag{14}$$

Outside the mitochondrion, the oxygen pressure drop associated with consumption varies as $1/r$ (Eq. 12). The spatial scale for the variation is the sphere radius a. For example, the drop has half its surface value for $r = 2a$.

The amplitude of the oxygen pressure drop is proportional to the consumption rate Γ and inversely proportional to the diffusivity K. The strongest parameter dependence is on the mitochondrial size, since $P_\bullet$ is proportional to a^2. Thus, doubling the size, for example, quadruples the drop in oxygen pressure.

To assess shape effects, we now consider the problem for a prolate spheroidal mitochondrion, with surface A given by

$$(x^2 + y^2)/b^2 + z^2/c^2 = 1. \tag{15}$$

Here b is the minor semi-axis and c is the major semi-axis. The calculations for the function $C(\mathbf{r})$, which are algebraically tedious, are summarized in the Appendix. The most important results can be expressed in terms of dimensionless shape factors S_C, S_A, and S_V. These are defined by

$$C_C = (3/2)P_\bullet S_C, \quad \langle C \rangle_A = P_\bullet S_A,$$

and

$$\langle C \rangle_V = (6/5)P_\bullet S_V \quad \text{(spheroid)}. \tag{16}$$

In these formulas, $P_\bullet$ is given by Eq. 13, where the volume of the spheroidal mitochondrion is $V = (4\pi/3)(b^2 c)$. The shape factor S_C is equal to the value of C_C for a spheroid divided by the value of C_C for a sphere of equal volume, and it is calculated directly from the solution for C given in the Appendix. S_A and S_V are defined and calculated in a similar way. Thus, the formulas (Eq. 16) reduce to the

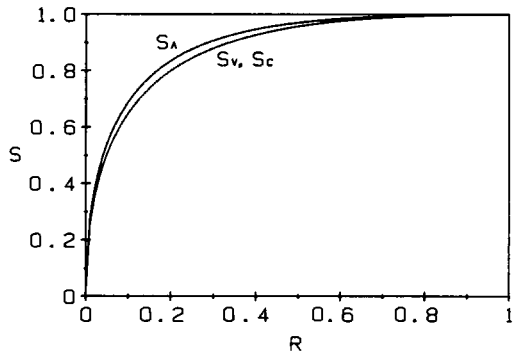

FIGURE 1 Shape factors for consumption gradients for prolate spheroidal mitochondria. R is the ratio of the minor axis to the major axis of the spheroid. Each shape factor is the ratio of an oxygen pressure drop for a spheroid to the same drop for a sphere of equal volume. The oxygen pressure drops are from infinity to the mitochondrial center (shape factor S_C), from infinity to the volume-averaged mitochondrial oxygen pressure (shape factor S_V), and from infinity to the surface-averaged mitochondrial oxygen pressure (shape factor S_A).

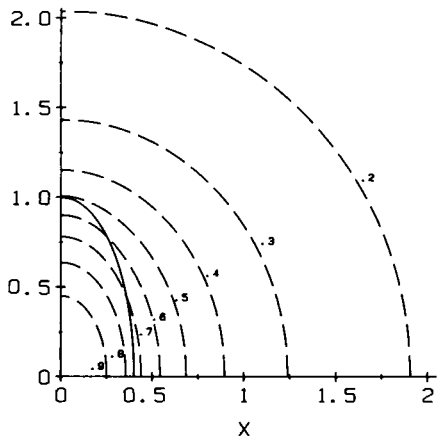

FIGURE 2 Contours of normalized oxygen pressure drop (dashed lines) around a spheroidal mitochondrion (solid line) of axis ratio $R = 0.4$. The length scale is chosen so that the major semi-axis is unity. The contours are for values of C/C_C, where C is the drop in oxygen pressure from infinity, and C_C is the value of C at the mitochondrial center. The contour for 0.1, which is off-scale, is nearly spherical, and has intercepts $z = 3.94$, $x = 3.88$. The contours are shown for one quadrant of any plane through the axis of symmetry of the mitochondrion; the contours in the other three quadrants are symmetric.

spherical case when each $S = 1$. The dimensionless shape factors are functions of the dimensionless spheroidal axis ratio

$$R = b/c. \tag{17}$$

Here $R = 1$ corresponds to a sphere, and $R = 0$ to a needle. Fig. 1 shows a plot of all three shape factors vs. R. The factors S_V and S_C are indistinguishable on this scale, and are only slightly less than S_A. The shape effects are not extremely large. We see, for example (from Fig. 1), that the replacement of a spheroid by a sphere of equal volume leads to an error of $<10\%$ for any axis ratio ≥ 0.5.

The spatial distribution of the oxygen pressure around and on the spheroid is somewhat difficult to characterize by a few numbers. Instead, we give in Fig. 2, by way of example, a contour plot for a spheroid of axis ratio $R = 0.4$. The contours are for constant values of C/C_C, a quantity that has a value of 1 at the mitochondrial center and 0 at infinity. The contours are less elongated than the mitochondrial surface, and the external contours become nearly spherical at a moderate distance from the mitochondrion. It is clear from the picture that the oxygen pressure varies on the mitochondrial surface: in this case, the surface variation is about one-quarter of the total variation from tissue to mitochondrial center.

Summary of Oxygen Variations

The oxygen pressure P is given in terms of C by Eq. 5. We can easily translate the results of Eq. 16 into terms of P, by using the facts that $\mathbf{F} \cdot \mathbf{r}$ has a 0 average over A and V, and vanishes at the mitochondrial center. We get

$$\begin{aligned} P_\infty - \langle P \rangle_A &= P_* S_A, \\ P_\infty - \langle P \rangle_V &= (6/5) P_* S_V, \end{aligned} \tag{18}$$

and

$$P_\infty - P_C = (3/2) P_* S_C.$$

Since the shape factors S_A, S_V, and S_C are all bounded by 1, we get simple upper bounds on the oxygen variations from Eq. 18 by replacing each S by 1. Although these bounds have been derived only for prolate spheroids, they probably are reasonably good for other convex shapes.

The drop in oxygen pressure from the local tissue value to the mitochondrial surface is given by

$$(\Delta P)_{MITO} = P_\infty - \langle P \rangle_A = P_* S_A. \tag{19}$$

It is of interest to compare this with the typical drop in oxygen pressure across an entire cell. The average volume rate of consumption of oxygen in the cell is given by $\Gamma_c = \Gamma F_m$, where F_m is the volume fraction of mitochondria. If we solve the steady state diffusion problem in the cell, $\nabla^2 P = \Gamma_c / K$, we can compute $(\Delta P)_{CELL}$, the drop in oxygen pressure from the average value on the cell boundary to the cell center. The result depends on the cell shape. For a cylindrical or spherical cell of radius R_c, we get

$$(\Delta P)_{CELL} = (\Gamma F_m / GK) R_c^2, \tag{20}$$

where $G = 4$ for a cylinder and 6 for a sphere. Then the ratio of the two drops is

$$(\Delta P)_{CELL} / (\Delta P)_{MITO} = (4\pi/3V)^{2/3} (3 F_m R_c^2 / G S_A). \tag{21}$$

Eq. 21 contains only geometric parameters. As we shall see in our later applications, we can use this equation to draw important conclusions that are independent of the values of the diffusivity K and the oxygen consumption rate Γ. The

meaning of the equation becomes more apparent if we drop numerical factors of order unity and look at the special case of a spherical mitochondrion of radius a:

$$(\Delta P)_{CELL}/(\Delta P)_{MITO} \sim F_m(R_c/a)^2. \quad (22)$$

In this form, we see the familiar quadratic dependence of the diffusive drops on the spatial scale.

APPLICATIONS

Skeletal Muscle

As our first example, we apply the theory to the case of skeletal muscle. We need values for the various parameters, and we begin with the tissue oxygen diffusivity D. This can be obtained from the experiments of Mahler (1978) on frog sartorius muscle. Mahler gives the value $D = 1.92 \times 10^{-5}$ cm^2/s at 37°C. Mahler also discusses the oxygen solubility coefficient, and we adopt the value he suggests, namely $B = 1.11 \times 10^{-9}$ mol/cm^3 · Torr for 37°C. These values give for the Krogh diffusivity $K = 2.13 \times 10^{-14}$ mol/cm · s · Torr. As Mahler discusses in detail, his values are very similar to values measured by other workers for other tissues—for example, Grote and Thews (1962) and Grote (1967) for rat myocardium, and Kawashiro et al. (1975) for rat abdominal muscle.

The mitochondrial geometric parameters needed are the volume V, the axis ratio R, and the mitochondrial volume fraction F_m. F_m is needed to convert measured whole tissue oxygen consumption rates to mitochondrial oxygen consumption rates. Values for these quantities are difficult to assign because mitochondrial shapes are sometimes very irregular, and because there is considerable heterogeneity in mitochondrial geometry, even within the same small tissue sample. Although a number of morphometric studies give values of F_m (e.g., Hoppeler et al., 1973, 1981), very few give values of the mitochondrial volume V and axis ratio R. One exception is the work of Wassilew and David (1977), comparing heart, diaphragm, and hindlimb muscle for dogs. Their results for the hindlimb muscle are particularly relevant, since shortly we will compare our theoretical results with the experiments of Gayeski et al. (1985) on dog gracilis muscle. Wassilew and David give the following values (±SD) for dog hindlimb muscle: volume, 0.8498 ± 0.5005 μm^3; length, 4.3276 ± 0.5033 μm; diameter, 0.4087 ± 0.0786 μm; volume fraction of mitochondria, 0.0845 ± 0.0265. These numbers present a problem. A prolate spheroid with dimensions equal to the mean length and diameter given would have a volume of 0.3785 μm^3, which is far smaller than the reported volume of 0.8498 μm^3. Even a circular cylinder with the given length and diameter has a volume of only 0.5677 μm^3. We make the tentative assumption that the volume, being a derived quantity, is more uncertain than the length and diameter. Thus, we use the mean length and diameter given by Wassilew and David, and we use the volume of a prolate spheroid with those dimensions. Then $R = (0.4087/4.3276) = 0.094$ for the axis ratio and $V = 0.38$ μm^3 for the volume. For the mitochondrial volume fraction, we also use Wassilew and David's number, $F_m = 0.085$.

Finally, consider the oxygen consumption rate. In experiments on dog gracilis muscle, Horstman et al. (1976) and Connett et al. (1985) find maximum oxygen consumption rates on the order of 0.15 ml/g · min. If we take a tissue density of 1.06 g/cm^3 (Mendez and Keys, 1960), then for $F_m = 0.085$, we get a maximum mitochondrial consumption rate of $\Gamma = 1.4 \times 10^{-6}$ mol/cm^3 · s.

With these parameter values, we can estimate the maximum drop in oxygen pressure from the nearby tissue to the surface-averaged mitochondrial value. From Fig. 1, we obtain, for $R = 0.094$, $S_A = 0.7$, $S_V = 0.65$, and $S_C = 0.65$. Then, from Eq. 18, we get $P_\infty - \langle P \rangle_A = 0.031$ Torr, $P_\infty - \langle P \rangle_V = 0.034$ Torr, and $P_\infty - P_c = 0.043$ Torr. One can understand why these numbers are so small on the basis of a geometric argument first pointed out by Gayeski (1981). The ratio of mitochondrial to capillary surface area in skeletal muscle is quite large—typically ~50 or more. In steady state, the same oxygen flux passes through both, so the local gradient at the mitochondrion is, on the average, only 1/50 (or less) of the gradient at the external capillary wall. Another geometric argument, leading to the same conclusion, can be based on Eq. 21. If we take a cylindrical cell of radius $R_c = 30$ μm, we get $(\Delta P)_{CELL}/(\Delta P)_{MITO} \approx 400$. Thus, perimitochondrial oxygen variations of more than a small fraction of a Torr would be associated with impossibly large cell-wide variations.

A few comments about the effect of myoglobin, which we have ignored so far, may be useful here. It is well known that myoglobin in skeletal muscle can affect oxygen delivery in two distinct ways: by storage of oxygen bound to the myoglobin and by facilitated transport (see, e.g., reviews by Kreuzer, 1970, Wittenberg, 1970, and Jacquez, 1984). In the steady state case considered here, only the facilitation mechanism is relevent. At high values of P_∞, any myoglobin present will be nearly saturated and will have little effect on transport. During heavy work, however, myoglobin buffers the oxygen pressure near the P_{50} for myoglobin (Gayeski et al., 1985; Connett et al., 1985), and facilitation can become important. We have investigated this by solving numerically the transport equations for spherical mitochondria, with myoglobin included in the surrounding tissue. Our results show that for myoglobin concentrations typical of dog gracilis (5×10^{-7} mol/cm^3), the drop in oxygen pressure is lower than the value calculated without myoglobin, by a factor that depends on P_∞. At high P_∞, there is no effect, but as $P_\infty \to 0$, the factor tends to ~0.5. This value of 0.5 is consistent with the experimental results of Wittenberg et al. (1975) and Cole (1982, 1983). Thus, myoglobin makes the perimitochondrial drops even smaller than the numbers given above.

It is of interest to compare our theoretical results with the recent experiments of Gayeski et al. (1985). They

measured oxygen distribution in dog gracilis muscle in a state of maximal oxygen consumption. The technique used was the determination of myoglobin saturation by cryospectrophotometry (described in detail by Gayeski, 1981). In a search for perimitochondrial oxygen variations, they used a spatial window of 2×3 μm. They found that such variations, calculated from myoglobin saturation, were below 0.15 Torr. This result is entirely consistent with the theory presented here. They also observed small values of $(\Delta P)_{CELL}$—typically <10 Torr. This, in combination with our above estimate that $(\Delta P)_{CELL}/(\Delta P)_{MITO} \sim 400$, gives $(\Delta P)_{MITO} \sim 0.025$ Torr, which is again consistent with theory.

Other relevant experiments include the work of Cole et al. (1982). They studied suspensions of rat skeletal muscle mitochondria, and they measured the oxygen consumption of the mitochondria as a function of the oxygen pressure in the suspending liquid. When consumption was not oxygen limited, they measured a mitochondrial consumption rate of $\Gamma \approx 1.3 \times 10^{-6}$ mol/cm^3 · s, which is very close to the value used in our calculations above. Since the oxygen diffusivity of their suspending liquid cannot be very different than the value we used (they are both of the same order of magnitude as the value for water), the conditions of their experiment are very similar to the in vivo situation that we have modeled. The oxygen pressure in their suspending liquid, which corresponds to our P_∞, is lowered until the oxygen consumption drops appreciably. The value K_M at which this happens is clearly an upper bound on the perimitochondrial oxygen drop. They found K_M to be in the range 0.02–0.05 Torr. This is in excellent agreement with our estimate of the perimitochondrial oxygen drops.

Hepatocyte Suspensions

We consider here the comparison of theory with the experiments of Jones and Kennedy (1982) on rat hepatocyte suspensions. These experiments are particularly important to analyze, because Jones and Kennedy have claimed very large perimitochondrial oxygen drops (of the order of 5 Torr) on the basis of their measurements. Experiments of this type are difficult to interpret. The problem is that the drop in oxygen pressure from the suspending medium to the mitochondrial cytochromes has several components: (*a*) from the bulk liquid to the cell surface (i.e., the unstirred layer); (*b*) from the cell surface to the cell interior; (*c*) from the cell interior to the mitochondrial surface; (*d*) from the mitochondrial surface to the mitochondrial interior. In the experiments of Jones and Kennedy, the oxygen pressure is measured in the bulk liquid and inferred for the mitochondrial interior from the observed state of the cytochromes. The experiment gives no direct information about how this total drop is distributed over the above four components. In the analysis of their data, Jones and Kennedy attributed the entire drop of ~5 Torr to component *c*. In the absence of a well-established value for the oxygen diffusivity for the hepatocyte interior, we cannot calculate the perimitochondrial drop directly. However, we can use Eq. 21 for $(\Delta P)_{CELL}/(\Delta P)_{MITO}$ to clarify the situation. Jones and Kennedy report a mitochondrial volume fraction $F_m = 0.12$, an ovoid shape, and a size of 0.6×1.5 μm. If we assume a prolate spheroid, then we find a volume $V = 0.28$ μm^3 and a shape factor (from Fig. 1) of $S_A = 0.95$. The hepatocytes are approximately spherical, with a volume of 7,250 μm^3 (Krebs et al., 1974), giving a radius $R_c = 12$ μm. Then Eq. 21, with $G = 6$, gives $(\Delta P)_{CELL}/(\Delta P)_{MITO} \sim 50$. Thus, the drop from cell edge to cell center is 50 times greater than the drop around each mitochondrion. A drop of ~5 Torr around each mitochondrion would be associated with an impossibly large variation of several hundred Torr across the cell. The conclusion is that the 5-Torr drop measured by Jones and Kennedy has its origin in heterogenity within the cell, and also in the unstirred layer around each cell. If, for example, the drop is divided equally between the unstirred layer and the cell interior, then the drop around each mitochondrion is only $2.5/50 = 0.05$ Torr, a number comparable to our earlier estimate for skeletal muscle. A more quantitative comparison of theory with cell suspension experiments will require a thorough analysis of all of the components of the oxygen pressure drop and also of values for the hepatocyte oxygen diffusivity. The simple arguments given here suffice to show that the perimitochondrial oxygen drops are very much smaller than the other oxygen drops in the diffusion path.

SUMMARY AND CONCLUSIONS

The oxygen distribution in tissue is best thought of as a superposition of a large-scale field and small-scale perturbations. The large-scale field varies on the scale of the cell and corresponds to the solution of the classical Krogh model. The small-scale perturbations are produced by oxygen-consuming mitochondria and have a scale of variation of a few microns. The perimitochondrial drop in oxygen pressure produced by consumption is of the order of $(\Gamma/3K)\ (3V/4\pi)^{2/3}$, where Γ is the rate of oxygen consumption per unit volume of mitochondrial tissue, V is the mitochondrial volume, and K is the Krogh oxygen diffusivity for the tissue outside the mitochondrion. These perimitochondrial oxygen variations, $(\Delta P)_{MITO}$, are much smaller than the cell-wide variations $(\Delta P)_{CELL}$. In order of magnitude, $(\Delta P)_{CELL}/(\Delta P)_{MITO} \sim F_m(R_c/a)^2$, where F_m is the volume fraction of mitochondria, R_c is the cell radius, and a is the mitochondrial radius.

The theory has been applied to two cases for which there are experimental data: skeletal muscle in vivo and hepatocyte suspensions. For maximally working skeletal muscle, we find perimitochondrial oxygen drops of only a few hundredths of a Torr. The treatment of the hepatocyte suspensions is somewhat less direct, since the oxygen diffusivity is not well known. By using the calculated result for $(\Delta P)_{CELL}/(\Delta P)_{MITO}$, we come to the same conclusion: the perimitochondrial drops are only a few hundredths of a

Torr. Bouwer and van den Thillart (1984) came to a similar conclusion from their calculations for suspensions of mitochondria from goldfish red muscle.

Finally, we return to the four questions raised in the introduction, which can now be answered. (*a*) The local drops in P_{O_2} around individual mitochondria are too small to be observed with presently available techniques. (*b*) The cytochromes in an isolated oxygen-consuming mitochondrion are exposed to a P_{O_2} only a few hundredths of a Torr lower than that of the nearby tissue. (*c*) The variations in P_{O_2} on the mitochondrial surface are comparable to the perimitochondrial drops and are thus only a few hundredths of a Torr. (*d*) In modeling oxygen transport to tissue, we can ignore individual mitochondria and just deal with a smoothed-out distribution of oxygen sinks.

APPENDIX

The solution of the boundary-value problem given by Eqs. 6–8 is easily obtained by a standard analysis, as given, for example, by Morse and Feshbach (1953, section 10.3) or by MacMillan (1958). Our purpose here is not to repeat the mathematical analysis, but to summarize the formulas needed to compute the shape factors and any other quantities associated with the oxygen distribution around a prolate spheroid.

Consider a prolate spheroid with foci at $x = y = 0$, $z = \pm f/2$. The distances to the foci from a point with Cartesian coordinates (x, y, z) are

$$r_1 = [x^2 + y^2 + (z + f/2)^2]^{1/2},$$

$$r_2 = [x^2 + y^2 + (z - f/2)^2]^{1/2}. \quad \text{(A1)}$$

Dimensionless prolate spheroidal coordinates ϵ, η, and ω are then defined by (Morse and Feshbach 1953):

$$\epsilon = (r_1 + r_2)/f, \quad \eta = (r_1 - r_2)/f, \quad \omega = \tan^{-1}(y/x). \quad \text{(A2)}$$

The ranges are $1 \le \epsilon < \infty$, $-1 \le \eta \le 1$, and $0 \le \omega < 2\pi$. The surface $\epsilon = \epsilon_A$ is a prolate spheroid with interfocal distance f, major semi-axis $c = \epsilon_A f/2$, and minor semi-axis $b = (\epsilon_A^2 - 1)^{1/2} f/2$. Thus, to get a spheroid with given b and c, we choose $f = 2(c^2 - b^2)^{1/2}$. Then the boundary is given by $\epsilon = \epsilon_A = (1 - b^2/c^2)^{-1/2}$. The axis ratio is $R = (b/c) = (1 - \epsilon_A^{-2})^{1/2}$. The surfaces η = constant are confocal hyperboloids of revolution. The formulas for the inverse transformation are

$$(x, y) = (f/2)\,[(\epsilon^2 - 1)(1 - \eta^2)]^{1/2}(\cos\omega, \sin\omega),$$

$$z = (f/2)\epsilon\eta. \quad \text{(A3)}$$

The Laplacian is given by

$$\nabla^2 C = \frac{4}{f^2(\epsilon^2 - \eta^2)}\left[\frac{\partial}{\partial\epsilon}(\epsilon^2 - 1)\frac{\partial C}{\partial\epsilon} + \frac{\partial}{\partial\eta}\cdot(1 - \eta^2)\frac{\partial C}{\partial\eta} + \frac{\epsilon^2 - \eta^2}{(\epsilon^2 - 1)(1 - \eta^2)}\frac{\partial^2 C}{\partial\omega^2}\right]. \quad \text{(A4)}$$

The volume element $d\tau$ is

$$d\tau = (f^3/8)(\epsilon^2 - \eta^2)\,d\epsilon\,d\eta\,d\omega, \quad \text{(A5)}$$

and the element of area $d\sigma$ on a surface ϵ = constant is

$$d\sigma = (f^2/4)\,[(\epsilon^2 - \eta^2)(\epsilon^2 - 1)]^{1/2}\,d\eta\,d\omega. \quad \text{(A6)}$$

The solutions of the Laplace and Poisson equations can be obtained in terms of Legendre functions (Morse and Feshbach, 1953). For our purposes, it is sufficient to give just the results of the calculations. We have

$$C = Q[A(\epsilon) + B(\epsilon)(3\eta^2 - 1)/2], \quad \text{(A7)}$$

where

$$Q = f^2\Gamma/K = 12[\epsilon_A(\epsilon_A^2 - 1)]^{-2/3}P_*. \quad \text{(A8)}$$

The functions $A(\epsilon)$ and $B(\epsilon)$ have different forms inside and outside the mitochondrion. Inside $(1 \le \epsilon \le \epsilon_A)$, we have

$$A(\epsilon) = A_I(\epsilon) = \alpha - \epsilon^2/24, \quad \text{(A9)}$$

and

$$B(\epsilon) = B_I(\epsilon) = \beta(3\epsilon^2 - 1)/2 - 1/36. \quad \text{(A10)}$$

Outside the mitochondrion $(\epsilon_A \le \epsilon)$ we have

$$A(\epsilon) = A_O(\epsilon) = (\gamma/2)\ln[(\epsilon + 1)/(\epsilon - 1)], \quad \text{(A11)}$$

and

$$B(\epsilon) = B_O(\epsilon) = (\delta/2)\{[3\epsilon^2 - 1)/2]\ln[(\epsilon + 1)/(\epsilon - 1)] - 3\epsilon\}. \quad \text{(A12)}$$

The four constants α, γ, β, and δ, obtained from the matching conditions (Eq. 7), are given by

$$\alpha = [\epsilon_A(\epsilon_A^2 - 1)/(24)]\ln[(\epsilon_A + 1)/(\epsilon_A - 1)] + (\epsilon_A^2/24), \quad \text{(A13)}$$

$$\gamma = \epsilon_A(\epsilon_A^2 - 1)/12, \quad \text{(A14)}$$

$$\beta = -(\epsilon_A^2 - 1)W/18, \quad \text{(A15)}$$

and

$$\delta = -\epsilon_A(\epsilon_A^2 - 1)/12, \quad \text{(A16)}$$

where

$$W = (3\epsilon_A/4)\ln[(\epsilon_A + 1)/(\epsilon_A - 1)] - 0.5(3\epsilon_A^2 - 2)/(\epsilon_A^2 - 1). \quad \text{(A17)}$$

The calculation of the shape factors defined in Eq. 16 requires the values of C_C, $\langle C\rangle_A$, and $\langle C\rangle_V$. The integrations for $\langle C\rangle_A$ and $\langle C\rangle_V$ are tedious but straightforward. We get

$$C_C = C(\epsilon = 1, \eta = 0) = Q(\alpha - \beta/2 - 1/36), \quad \text{(A18)}$$

$$\langle C\rangle_A = \left(\int\int C\,d\sigma\right)\Big/\left(\int\int d\sigma\right) = Q[A_I(\epsilon_A) + gB_I(\epsilon_A)], \quad \text{(A19)}$$

where

$$g = \frac{[\epsilon_A^2(3\epsilon_A^2 - 4)\sin^{-1}(1/\epsilon_A) - (3\epsilon_A^2 - 2)(\epsilon_A^2 - 1)^{1/2}]}{8[\epsilon_A^2\sin^{-1}(1/\epsilon_A) + (\epsilon_A^2 - 1)^{1/2}]}, \quad \text{(A20)}$$

and

$$\langle C\rangle_V = \left(\int\int\int C\,d\tau\right)\Big/\left(\int\int\int d\tau\right) = Q(\alpha - \beta/5 - \epsilon_A^2/40 - 1/90). \quad \text{(A21)}$$

The three shape factors S_C, S_A, and S_V can now be calculated from Eqs. 14, 17, A8, A13, A15, and A18–A21.

We thank Professors R. J. Connett, T. E. J. Gayeski, and C. R. Honig for their continuing interest in this analysis, for their helpful suggestions, for sharing their data, for many stimulating discussions, and for their detailed comments on the manuscript. We thank Professors G. R. Cokelet and I. H. Sarelius for listening critically to various versions of this work. We thank the referees for their useful suggestions. We are grateful to Professor P. L. LaCelle and the Dept. of Radiation Biology and Biophysics for providing a haven in the University of Rochester Medical School during the 1984–85 year.

This work was supported in part by National Institutes of Health grant HL-18208.

Received for publication 3 June 1985.

REFERENCES

Bouwer, S., and G. van den Thillart. 1984. Oxygen affinity of mitochondrial state III respiration of goldfish red muscles: the influence of temperature and O_2 diffusion on K_m values. *Mol. Physiol.* 6:291–306.

Cole, R. P. 1982. Myoglobin function in exercising skeletal muscle. *Science (Wash. DC).* 216:523–525.

Cole, R. P. 1983. Skeletal muscle function in hypoxia: effect of alteration of intracellular myoglobin *Respir. Physiol.* 53:1–14.

Cole, R. P., P. C. Sukanek, J. B. Wittenberg, and B. A. Wittenberg. 1982. Mitochondrial function in the presence of myoglobin. *J. Appl. Physiol. Respir. Environ. Exercise Physiol.* 53:1116–1124.

Connett, R. J., T. E. J. Gayeski, and C. R. Honig. 1985. An upper bound on the minimum P_{O_2} for O_2 consumption in red muscle. *Adv. Exp. Med. Biol.* In press.

de Koning, J., L. J. C. Hoofd, and F. Kreuzer. 1981. Oxygen transport and the function of myoglobin: theoretical model and experiments in chicken gizzard smooth muscle. *Pfluegers Arch. Eur. J. Physiol.* 389:211–217.

Fletcher, J. E. 1980. On facilitated oxygen diffusion in muscle tissues. *Biophys. J.* 29:437–458.

Gayeski, T. E. J. 1981. A cryogenic microspectrophotometric method for measuring myoglobin saturation in subcellular volumes; application to resting dog gracilis muscle. Ph.D. thesis. University of Rochester, Rochester, NY.

Gayeski, T. E. J., R. J. Connett, and C. R. Honig. 1985. O_2 transport in the rest–work transition illustrates new functions for myoglobin. *Am. J. Physiol.* 248:H914–H921.

Grote, J. 1967. Die Sauerstoffdiffusionskonstanten im Lungengewebe and Wasser und ihre Temperaturabhängigkeit. *Pfluegers Arch. Eur. J. Physiol.* 295:245–254.

Grote, J., and G. Thews. 1962. Die Bedingungen für die Sauerstoffversorgung des Herzmuskelgewebes. *Pfluegers Arch. Eur. J. Physiol.* 276:142–165.

Hoppeler, H., P. Lüthi, H. Claassen, E. R. Weibel, and H. Howald. 1973. The ultrastructure of the normal human skeletal muscle. *Pfluegers Arch. Eur. J. Physiol.* 344:217–232.

Hoppeler, H., O. Mathieu, R. Krauer, H. Claassen, R. B. Armstrong, and E. R. Weibel. 1981. Design of the mammalian respiratory system. VI. Distribution of mitochondria and capillaries in various muscles. *Respir. Physiol.* 44:87–111.

Horstman, D. H., M. Gleser, and J. Delehunt. 1976. Effects of altering O_2 delivery on V_{O_2} of isolated working muscle. *Am. J. Physiol.* 230:327–334.

Jacquez, J. A. 1984. The physiological role of myoglobin: more than a problem in reaction-diffusion kinetics. *Mathematical Biosci.* 68:57–97.

Jones, D. P., and F. G. Kennedy. 1982. Intracellular oxygen supply during hypoxia. *Am. J. Physiol.* 243:C247–C253.

Kawashiro, T., W. Nüsse, and P. Scheid. 1975. Determination of diffusivity of oxygen and carbon dioxide in respiring tissue: results in rat skeletal muscle. *Pfluegers Arch. Eur. J. Physiol.* 359:231–251.

Krebs, H. A., N. W. Cornell, P. Lund, and R. Hems. 1974. Isolated liver cells are experimental material. *In* Regulation of Hepatic Metabolism. F. Lundquist and N. Tygstrup, editors. Academic Press, Inc., New York. 726–750.

Kreuzer, F. 1970. Facilitated diffusion of oxygen and its possible significance: a review. *Respir. Physiol.* 9:1–30.

Kreuzer, F., and L. Hoofd. 1984. Facilitated diffusion of oxygen: possible significance in blood and muscle. *Adv. Exp. Med. Biol.* 169:3–21.

Krogh, A. 1922. Anatomy and Physiology of Capillaries, Yale University Press, New Haven.

MacMillan, W. D. 1958. The Theory of the Potential. Dover, New York.

Mahler, M. 1978, Diffusion and consumption of oxygen in the resting frog sartorius muscle. *J. Gen. Physiol.* 71:533–557.

Mendez, J., and A. Keys. 1960. Density and composition of mammalian muscle. *Metabolism.* 9:184–188.

Morse, P. M., and H. Feshbach. 1953. Methods of Theoretical Physics. McGraw-Hill Inc., New York.

Tamura, M., N. Oshino, B. Chance, and I. A. Silver. 1978. Optical measurements of intracellular oxygen concentration of rat heart in vitro. *Arch. Biochem. Biophys.* 191:8–22.

Wassilew, G., and H. David. 1977. Vergleichende morphometrische Untersuchungen an normalen Herz- und Zwerchfellmitochondrien des Hundes. *Verh. Anat. Ges.* 71:239–241.

Wittenberg, J. B. 1970. Myoglobin-facilitated oxygen diffusion: role of myoglobin in oxygen entry into muscle. *Physiol. Rev.* 50:559–636.

Wittenberg, J. B., B. A. Wittenberg, and P. R. B. Caldwell. 1975. Role of myoglobin and the oxygen supply to red skeletal muscle. *J. Biol. Chem.* 250:9038–9043.